

Realistic prediction of post-cracking behavior for new structural synthetic fiber reinforced concrete beams

B.H.Oh, J.C.Kim, D.K.Park, Y.C.Choi

Professor & Research Assistants, Dept. of Civil Engineering, Seoul National University

San 56-1, Shinrim-dong, Gwanak-ku, Seoul, Korea

ABSTRACT : A realistic method of analysis for the post-cracking behavior of newly-developed structural synthetic fiber reinforced concrete beams is proposed. In order to predict the post-cracking behavior, pullout behavior of single fiber is identified by tests and employed in the model in addition to the realistic stress-strain behavior of concrete in compression and tension. A probabilistic approach is used to calculate the effective number of fibers across crack faces and to calculate the probability of non-pullout failure of fibers. The proposed theory is compared with test data and shows good agreement. The proposed theory can be efficiently used to predict the load-deflection behavior, moment-curvature relation, load-crack mouth opening width (CMOD) relation of synthetic fiber reinforced concrete beams.

Keywords : structural synthetic fiber, post-cracking behavior, FRC beams, cracking, fiber pull-out test

1 INTRODUCTION

Fibers have been used in many areas of concrete structures including tunnel linings, impact-resistant structures, and repair/rehabilitation of damaged structures. However, most important application of fibers would be to prevent or control the tensile cracking occurring in concrete structures (Gopalaratnam and Shah 1985, Soroushian & Lee 1990, Oh 1992, Ezeldin et al. 1992, Bantia & Trottier 1994, Leung & Geng 1998, Li et al. 1998, Nataraja et al. 1999, Oh 2002). It is, therefore, necessary to model realistically the post-cracking behavior of fiber-reinforced concrete members.

Recently, structurally-efficient synthetic fibers have been developed by authors and coworkers (Oh, et al 2002). These synthetic fibers have advantages compared to steel or other fibers in that they are corrosion-resistant and exhibit high energy-absorption capacity.

The purpose of the present study is to explore experimentally and theoretically the cracking resistance and post-cracking behavior of newly-developed structural synthetic fiber reinforced concrete beams. To this end, the pullout tests of fibers were executed which simulate pullout behavior of fibers at crack surfaces. The arbitrarily-oriented fibers at the crack surface have been considered by introducing a probabilistic concept. The load-deflection and moment-curvature curves were generated from the theory derived in this study and compared with test data.

2 MODELS FOR POST-CRACKING BEHAVIOR

2.1 *Concept of analysis*

A fiber reinforced concrete beam as shown in Figure 1 has been considered for the analysis of post-cracking behavior. Figure 1 shows the failure mode of a beam with the crack mouth opening displacement. Figure 2 depicts the strain and stress distributions along the depth of normal reinforced concrete(RC) beam. These stress distributions can be redrawn as shown in Figure 3 for fiber-reinforced concrete(FRP) beams. In this Figure 3, the pullout forces of fibers in tensile region depend on the crack opening displacements along the depth from neutral axis.

In order to obtain the post-cracking behavior of FRC beams, the stress-strain relations of concrete in compression and tension, and the stress-crack width relation after cracking must be properly defined. This will be clarified in the next section.

2.2 *Stress-strain relation of concrete in compression*

The Hognestad's stress-strain relation(Equation 1 and Equation 2) of concrete in compression is employed in this study, which is one of the most-generally used equation to model the constitutive behavior of concrete. Figure 4 exhibits the typical stress-strain relation of concrete in compression.

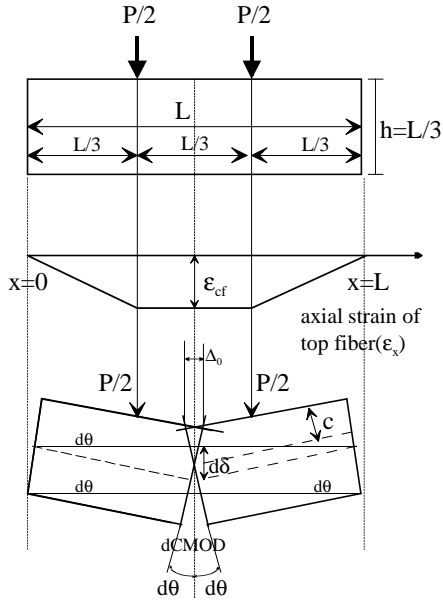


Figure 1. Failure mode of FRC beam under load

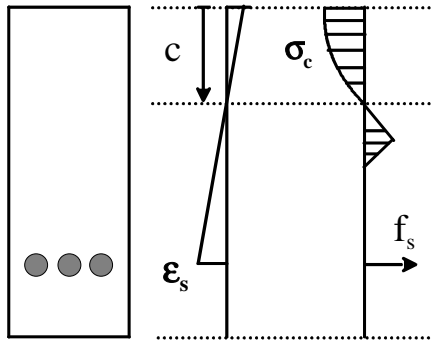


Figure 2. Stress and strain relation of RC beam

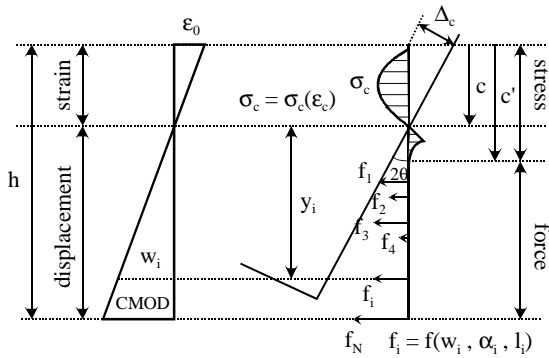


Figure 3. Schematic view of forces and stresses acting on cracked section of FRC beam.

$$f_c = f_c' \left[2 \frac{\epsilon_c}{\epsilon_0} - \left(\frac{\epsilon_c}{\epsilon_0} \right)^2 \right] \text{ for } 0 \leq \epsilon_c \leq \epsilon_0 \quad (1)$$

$$f_c = f_c' \left[1 - \frac{0.15}{0.004 - \epsilon_0} (\epsilon_c - \epsilon_0) \right]$$

$$\text{for } \epsilon_0 \leq \epsilon_c \leq 0.003 \quad (2)$$

in which f_c' = compressive strength of concrete, ϵ_0 = the strain at peak stress (see Figure 4). The force C in compression zone can be written as follows.

$$C = \alpha f_c' b c \quad (3)$$

where α = the factor for average stress, b = width of beam, and c = the depth of neutral axis from the top face of a beam. The factor α can be considered as a conversion factor from actual stress-strain curves to a rectangular stress block. This can be obtained by equating the area under actual stress-strain curve to the area under rectangular stress block as follows (Park & Paulay 1975)

$$\int_0^{\epsilon_{cf}} f_c d\epsilon_c = \alpha f_c' \epsilon_{cf} ; \text{ Then } \alpha = \frac{\int_0^{\epsilon_{cf}} f_c d\epsilon_c}{f_c' \epsilon_{cf}} \quad (4)$$

The location of the compression force, γ , from the top fiber can be obtained as

$$\gamma = 1 - \frac{\int_0^{\epsilon_{cf}} \epsilon_c f_c d\epsilon_c}{\epsilon_{cf} \int_0^{\epsilon_{cf}} f_c d\epsilon_c} \quad (5)$$

where γ = centroid factor for compression force.

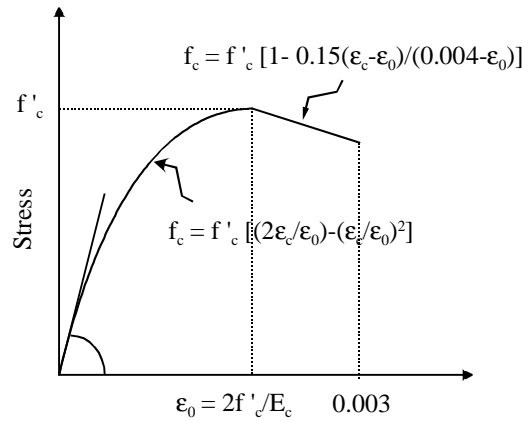


Figure 4. Hongnstad's stress-strain curve for concrete in compression

2.3 Stress-strain relation of concrete in tension

2.3.1 Tensile behavior before crack occurrence

The tensile behavior of concrete can be reasonably assumed as linear elastic before cracking. The elastic modulus is generally described as

$$E_{ct} = 5500\sqrt{f_c'} \quad (\text{MPa}) \quad (6)$$

2.3.2 Post-cracking behavior of concrete after tensile strength

The cracking starts to occur right after the tensile stress reaches the tensile strength and the tensile stress decreases as the crack width increases. The strain at first cracking, ϵ_{cr} , can be obtained as follows.

$$\epsilon_{cr} = \frac{f_r}{E_{ct}} \quad (7)$$

in which f_r = tensile strength of concrete, E_{ct} = elastic modulus before cracking.

The stresses after cracking depend on the widths of cracks. It is reasonably written here based on the Gopalotratnam & Shah's model (1985)[see Figure5].

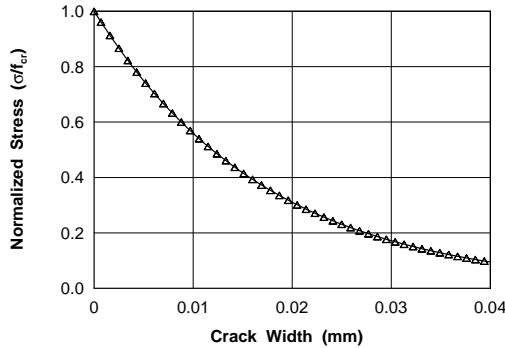


Figure 5. Tension softening curve after cracking (Shah's model)

$$\frac{\sigma_{ct}}{f_c} = e^{-kw\lambda} \quad (8)$$

in which σ_{ct} = the tensile stresses after cracking, k = empirical constant = 60.8, w = crack width(in mm), λ = empirical constant = 1.01.

2.4 Calculation of sectional forces and deflections of FRC beams

The deformation of concrete beams without reinforcing bars is usually localized at central position as shown in Figure 1. The cracked portion at central location acts as a plastic hinge.

The distribution of compressive strain at extreme fiber of the beam, ϵ_x , is shown in Figure 1(b). The displacement Δ_n at compression face can be obtained from this compressive strain distribution ϵ_x .

$$\Delta_0 = \int_0^L \epsilon_x dx = \epsilon_{cf} \frac{2}{L} \quad (9)$$

The slope(rotation angle) of beam, $d\theta$, may also be obtained from Figure 1.

$$d\theta \approx \frac{\Delta_0}{2c} \quad (10)$$

The deflection at central position is obtained from the slope of the beam as follows.

$$d\delta = d\theta \frac{L}{2} \quad (11)$$

The crack mouth opening displacement (CMOD) at the bottom surface is also written as

$$dCMOD = 2[d\theta(h-c)] \quad (12)$$

The internal resisting moment, M_e , of the beam can be derived from the stress distributions of concrete in compression and tension zones and also the pullout forces of all the fibers across the crack plane as shown in Figure 3(Equation 13 and 14).

$$\int_0^c \sigma_c (bd y) + \sum_{i=1}^N f_i = 0 \quad (13)$$

$$M_e = \int_0^c \sigma_c bdy \cdot y + \sum_{i=1}^N (f_i y_i) \quad (14)$$

From the moment of Equation 14, the applied load on the beam, P , is obtained as follows.

$$P = \frac{6M_e}{L} \quad (15)$$

The pullout force f_i of the fiber of i^{th} layer in Equation 14 should be obtained from the relation of bond stress and bond slip of a fiber and they directly depend on the crack widths of the beam(see Equation 16).

$$w_i = \left[\frac{CMOD}{(h-c)} \right] y_i \quad (16)$$

The fibers are randomly distributed at the crack plane as shown in Figure 6 and this effect must be considered appropriately to calculate the fiber

forces. Bantia(1994) reported that the average number of fibers per unit area of crack plane follows normal distribution and can be summarized depending on the fiber contents as shown in Table 1.

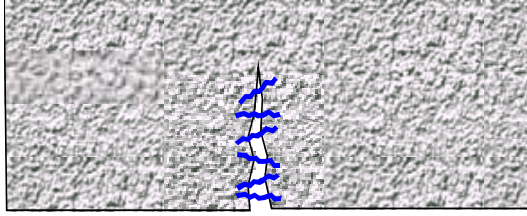


Fig. 6 Orientation and embedded length of randomly distributed fibers

Table 1. Average number of fibers according to fiber content

Fiber content, percent of volume	0.75%	1.50%
Average, fibers per 4cm ²	7.922	15.173
Standard deviation, fibers per 4cm ²	6	8.9
Sample size, n	448	493

On the other hand, Soroushian and Lee(1990) proposed the number of fibers per unit area, N_1 , as follows.

$$N_1 = \alpha \frac{V_f}{A_f} \quad (17)$$

where, α = fiber orientation factor, V_f = fiber content, and A_f = cross-sectional area of fibers.

The orientation factor α can be considered as the effective factor that an arbitrary-oriented fiber is perpendicular to the crack plane(see Figure7).

$$\alpha_0 = \frac{\int_0^{\pi/2} \int_0^{\pi/2} l_f \cos \theta \cos \psi d\theta d\psi}{\left(\frac{\pi}{2}\right)^2 l_f} = 0.405 \quad (18)$$

If the boundary of the structure restrains the arbitrary orientation of the fibers, the orientation factor for a specified direction becomes larger. Soroushian and Lee(1990) reported the orientation factor for two-side-restrained case as follows.

$$\alpha_1 = \frac{\int_{d_f/2}^{h/2} \beta_1 dy}{h/2} \quad \text{for } h < l_f \quad (19)$$

$$\alpha_1 = \frac{l_f \int_{d_f/2}^{l_f/2} \beta_1 dy}{hl_f/2} + 0.405(1 - l_f/h) \quad (20)$$

$$\text{where } \beta_1 = \frac{\int_0^{\pi/2} \int_{r_0}^r l_f \cos \theta \cos \psi d\theta d\psi}{l_f(\pi/2)r} \quad (21)$$

$$\text{with } r_0 = \sin^{-1}(d_f/l_f) \text{ and } r = \sin^{-1}(2y/l_f) \quad (22)$$

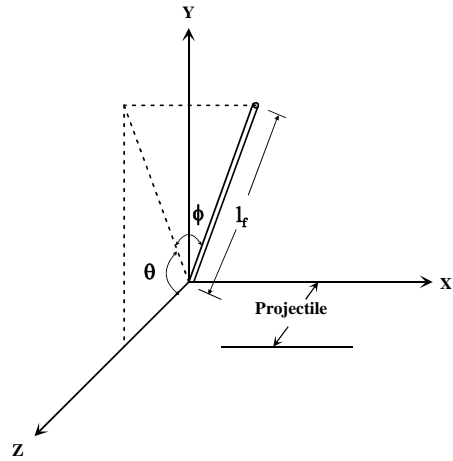


Figure 7. Three-dimensional fiber orientation

The tensile force(F_i) resisted by fibers at each layer of tensile zone of the beam can be obtained by multiplying the fiber force f_i of that layer by the number of fibers. The force f_i of single fiber can be derived from the bond stress-slip relation, which is also dependent upon the crack width w_i of i^{th} layer(see Figure 3). This bond stress-slip relation of structural synthetic fiber will be directly obtained by tests, which will be described in the following section.

The development length L_f of a fiber required for not to be pulled out at the crack plane may be derived as shown in Equation 23.

$$L_f = \frac{f_i}{\Sigma_0 \tau_u} \quad (23)$$

in which Σ_0 = perimeter of a fiber, and τ_u = bond strength of a fiber. Therefore, the actual embedment length of fibers should be larger than the required development length in order not to be pulled out.

Figure 8 summarizes the fiber forces, required anchorage lengths, and the probabilities of non-anchorage failure for various layers of cracked section of a beam. The probability of non-anchorage(or non-pullout) failure P_r can be derived as follows by two cases.

(1) Case 1 : Required anchorage length \leq the half of fiber length ($L_r \leq l_f/2$)

Figure 9 represents the cracked region of a beam. This is the case that the half of the actual fiber length (the region B in Figure 9(a)) is larger than the required anchorage length (the region A in Figure 9(a)). This can be written in a formalized equation as follows.

$$P_r = \frac{\text{area of B}}{\text{total area A and B}} = 1 - \frac{\text{area of A}}{\text{total area A and B}} \quad (24)$$

$$= 1 - \frac{(h-c)L_t/2}{(h-c)l_f/2} = 1 - \frac{L_t}{l_f}$$

(2) Case 2 : Required anchorage length $>$ the half of fiber length ($L_r > l_f/2$)

This is the case of Figure 9(b) that the required anchorage length is larger than the half of actual fiber length. This can be expressed as the following equation.

$$P_r = \frac{\text{area of region B}}{\text{total area of rectangle}} = \frac{(l_f/2)k/2}{(h-c)l_f/2} \quad (25)$$

$$= \frac{1}{2} \frac{l_f/2}{L_t} = \frac{1}{4} \frac{l_f}{L_t}$$

in which $k = \frac{l_f}{2}(h-c)/L_t$ (see Figure 9).

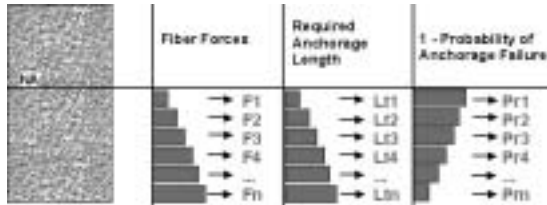


Fig. 8 Fiber force, required anchorage length, and probability of non-anchorage failure

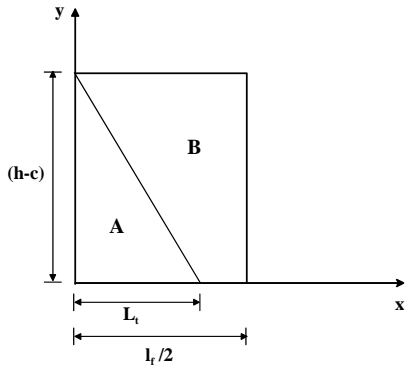


Fig. 9(a) Relation between required anchorage and embedded fiber length ($L_r \leq l_f/2$)

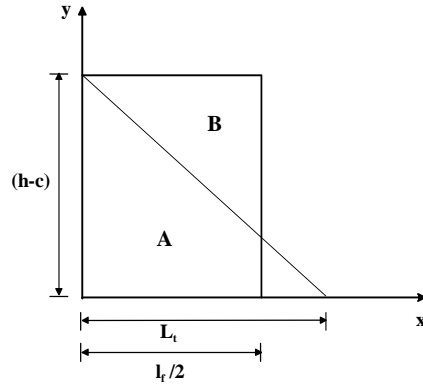


Fig. 9(b) Relation between required anchorage and embedded fiber length ($L_r > l_f/2$)

Finally, the tensile forces resisted by fibers can be obtained from the number of fibers at each layer, effective orientation factor α , and the probability of non-anchorage failure P_r . The flow diagram for the flexural analysis of synthetic fiber-reinforced concrete beams is summarized in Figure 10.

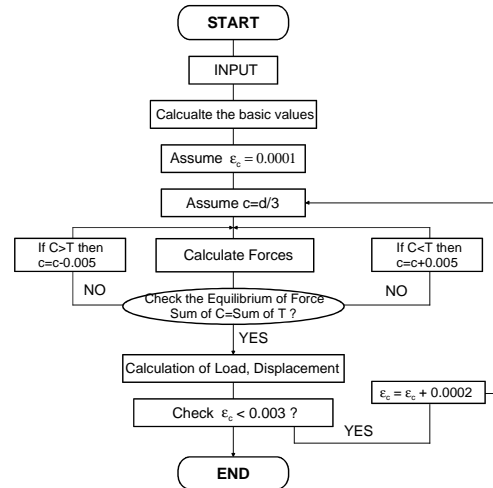


Figure 10. Flowchart for the analysis of synthetic FRC beams

3 TESTS FOR POST-CRACKING BEHAVIOR OF STRUCTURAL SYNTHETIC FRC BEAMS

3.1 Pullout test for single fiber

The authors developed recently new structural synthetic fibers which are of crimped type with the length of 50mm. Figure 11 shows the pullout test specimen specially prepared for obtaining the pullout load-slip relation. Figure 12 shows the photograph for actual pullout test arrangement.

Figure 13 depicts the average pullout load versus slip relation obtained from the present tests. The bond load-slip equation obtained from the tests may have the following form.

$$F_p = \frac{aS}{b+cS^d} \quad (26)$$

where a, b, c, and d are the constants to be obtained from test data, and F_p = pullout load(kN), S = slip in mm unit.

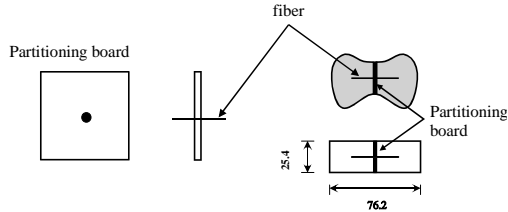


Figure 11. Pullout test specimen



Figure 12. Photograph of pullout test

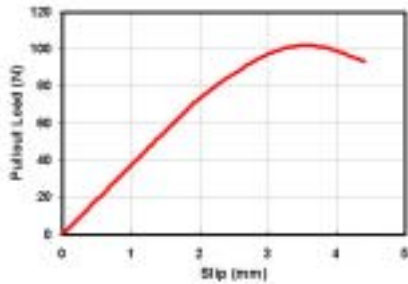


Figure 13. Load-slip relation for crimped-type synthetic fiber

3.2 Flexural tests for structural synthetic fiber reinforced concrete beams

The concrete beams reinforced with structural synthetic fibers have been tested to obtain the flexural behavior including the load-deflection behavior, load-CMOD relations, and moment-curvature relations. The mixture proportion of concrete is summarized in Table 2. The water-cement ratio was 0.45 and the fiber content was 1 percent of total concrete volume. The mixture was designed to accommodate the use for tunnel shotcrete lining structures.

Table 2. Mixture proportion for test specimens

W/C (%)	Unit Weight(kg/m ³)				Fiber Content (1%)
	Cement	Water	Sand	Gravel	
45	453	204	1115	487	9

Figure 14 exhibits the arrangement for flexural tests of fiber reinforced concrete beams in four-point loading condition. Figure 15 show special measuring device for central deflection of the beam. This device allows to measure exact relative displacements between the supports and center point.

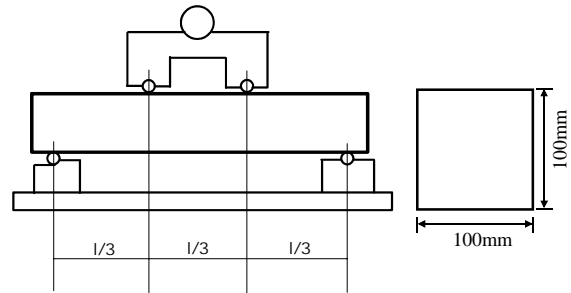


Figure 14. Schematic view of flexural tests

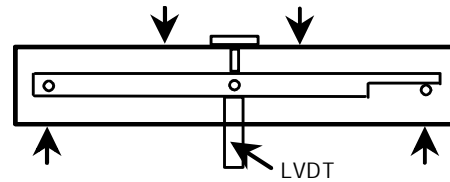


Figure 15. Devices for displacement measurement

The dimension of the beam was 100×100×400mm and the span length was 300mm. The load was applied in displacement control manner with the rate specified in the static testing standard.

4 ANALYSIS OF TEST RESULTS AND COMPARISONS WITH THEORY

Figure 16 shows the load-deflection curves obtained from the present tests for the beam with structural synthetic fiber volume of 1 percent. Figure 16 also compares the test data with the theory proposed in the previous section. It can be seen that the theoretical predictions fairly well agree with test data even after post-cracking ranges.

The salient feature of the post-cracking behavior of structural synthetic fiber reinforced concrete beams is that the resisting load drops down right after first cracking, probably due to initial slip of fibers at crack plane, and then starts to increase due to structurally effective synthetic fibers in tensile region. Figure 17 also exhibits the

similar behavior of structural synthetic fiber reinforced concrete beam for fiber volume of 1.5%. It is seen again in Figure 17 that the proposed theory agrees very well with the measured data, even up to the large deflection of the beam.

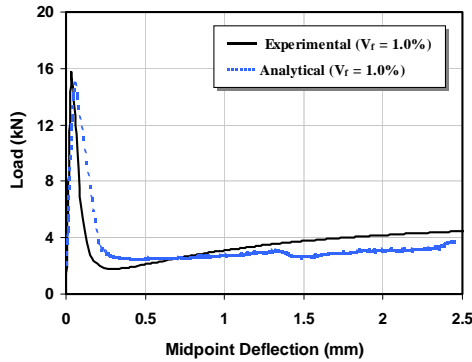


Figure 16. Load-deflection curve for structural synthetic fiber concrete beam (fiber content: $V_f = 1.0\%$ by volume)

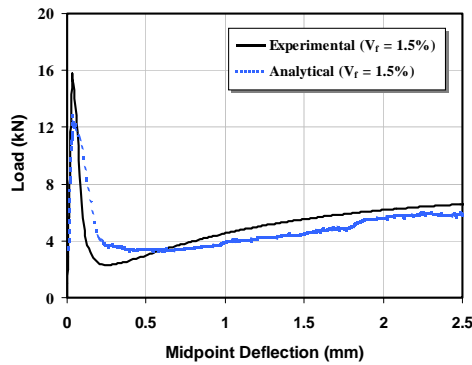


Figure 17. Load-deflection curve for structural synthetic fiber concrete beam (fiber content: $V_f = 1.5\%$ by volume)

Figure 18 shows the comparison of load-deflection behavior for two different fiber volume contents. Figure 18 indicates that the FRC beam with larger volume of fiber content (namely 1.5% by volume) exhibits higher resistance especially after larger deflection.

Figure 19 describes the load-CMOD relations for two different fiber volume contents. It is noted here that, at the same loads after cracking, the FRC beam with larger volume of fibers exhibits much smaller CMOD values. This is indeed a great beneficial effect of structural synthetic fibers. Figure 20 shows the relation between CMOD and central deflection of FRC beam. These relations are very much similar for different fiber volume contents. Therefore, this relation of CMOD versus central displacement may be regarded as a material property for structural synthetic fiber reinforced concrete beam.

Figure 21 shows the change of neutral axis depth according to central deflection. It is seen that the neutral axis depth continuously decreases, which reflects the crack growth according to the increase of applied load. Figure 22 describes the moment-curvature relations for FRC beams with two different fiber volumes. These curves are very similar to load-deflection curves previously described for synthetic fiber reinforced concrete beams

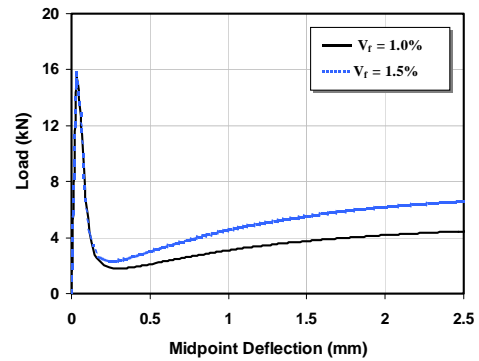


Figure 18. Effect of fiber content on load-deflection curves

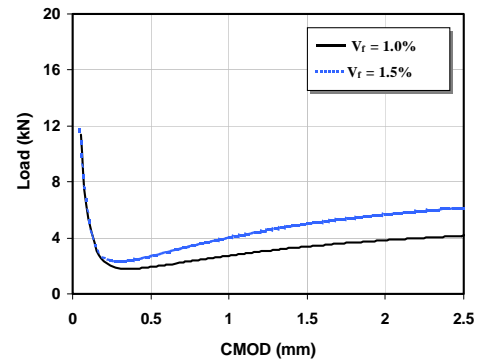


Figure 19. Effect of fiber content on load-CMOD relation

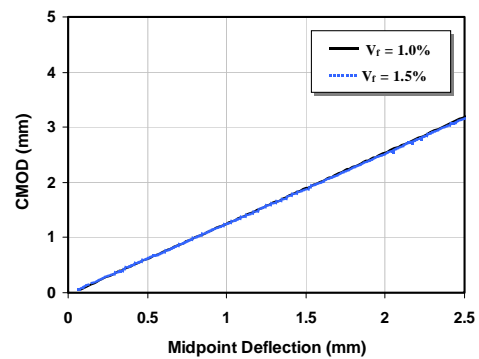


Figure 20. Relation between CMOD and deflection

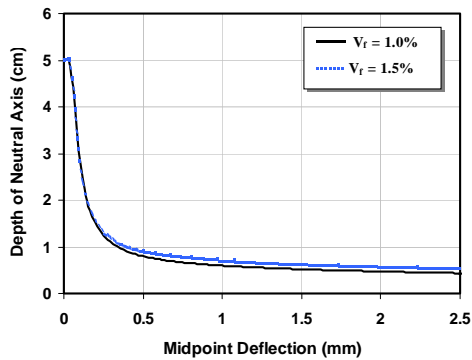


Figure 21. Variation of neutral axis depth according to the increase of deflection

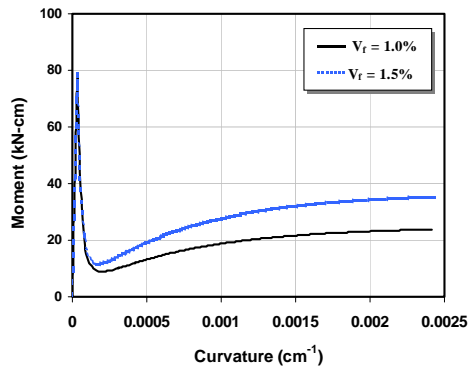


Figure 22. Prediction of Moment and curvature relation

5 CONCLUSIONS

The post-cracking behavior of concrete beams reinforced with recently-developed structural synthetic fibers is investigated in the present study. In order to develop a realistic model for post-cracking behavior of structural synthetic FRC beams, the randomness of orientation of fibers and the effective number of fibers at the crack plane were first considered and then new concept of the probability of non-pullout failure of fibers at the crack plane was introduced and derived in this study.

In order to calculate the pullout forces of structural synthetic fibers at the crack plane, the pullout tests for fibers were also conducted and an appropriate relation between bond forces and slips was derived. All these models were incorporated to formulate a method for flexural analysis of structural synthetic FRC beams.

The present tests for structural synthetic FRC beams indicates that the resisting load drops down right after the peak load and then starts to increase continuously due to the resistance of structural synthetic fibers. The theory developed in this study describes well these phenomena observed in the tests.

The load-CMOD relation, CMOD-deflection,

and moment-curvature relation were also reasonably predicted by the proposed theory. The present study indicates that the FRC beams with larger amount of fibers exhibits much smaller CMOD values at the same applied loads, which is one of the great beneficial effects of newly developed structural synthetic fibers. The present study also indicates that the relation between CMODs and central displacements is almost same for the beams with different fiber volumes and, therefore, this relation can be regarded as a material property for structural synthetic fiber reinforced concrete members.

The present study allows more realistic analysis and application of recently-developed structural synthetic fiber reinforced concrete beams.

6 REFERENCES

- ACI Committee 544, *Design Considerations for Steel Fiber Reinforced Concrete*
- ASTM C 1018-89, Standard Test Method for *Flexural Toughness and First-Crack Strength of Fiber Reinforced Concrete (Using Beam with Third-Point Loading)*, 1991 Book of ASTM Standards, V. 04.02, ASTM, Philadelphia: 507-513.
- Banithia, N. & Trottier, J. 1994. Concrete Reinforced with Deformed Steel Fibers, Part I : Bond-Slip Mechanism, *ACI Material Journal*, V. 91, No. 5, Sept.-Oct.: 435-446.
- Ezeldin, A.S. & Balaguru, P.N. 1992. Normal and High Strength Fiber Reinforced Concrete under Compression, *Journal of Materials in Civil Engineering*, 4(4): 415-427
- Gopalratnam, V.S. & Shah, S.P. 1985. Softening Response of Plain Concrete in Direct Tension, *ACI Journal*, Proceeding V. 82, No. 3, Mar.: 310-323
- Gopalratnam, V.S. et. al. and Wecharatana, M. 1991. Fracture Toughness of Fiber reinforced Concrete, *ACI Materials Journal*, V. 88, No. 4, July-Aug.: 339-353
- Lange-Kornbam, D. & Karihaloo B.L. 1997. Tension Softening of Fibre-Reinforced Cementitious Composites, *Cement and Concrete Composites* 19: 315-328
- Leung, C., Geng, Y.P. 1998. Micromechanical Modeling of Softening Behavior In Steel Fiber Reinforced Cementitious Composites, *Int. J. Solids Structures*, Vol. 35, No 31-32: 4205-4222.
- Nataraja, M.C. et al. 1999. Stress-strain curves for steel -fiber reinforced concrete under compression, *Cement & Concrete Composites* 21: 383-390
- Oh, B.H. 1992. Flexural analysis of reinforced concrete beams containing steel fibers, *ASCE, Journal of Structural Engineering*, 118(10): 2691-8.
- Oh, B.H. 2002. Cracking and flexural behavior of structural synthetic fiber reinforced concrete beams, *KCI Journal*, Vol. 14, No 6 : 900-909
- Park, R. & Paulay. T. 1975. *Reinforced concrete structures*. John Wiley and Sons, Inc., New York, N.Y.
- Romualdi, J.P. & Mandel, J. A. 1964. Tensile Strength of Concrete as Affected by uniformly Distributed and Closely Spaced Short Lengths of wire Reinforcement, *ACI Journal*, Proceedings V.61, No 6, June: 650-670.
- Soroushian, P. & Lee, C. 1990. Distribution and Orientation of Fibers in Steel Fiber Reinforced Concrete, *ACI Material Journal*, V. 87, No. 5, Sep.-Oct.: 433-439
- Soroushian, P. & Lee, C. 1990. Tensile Strength of Steel Fiber Reinforced Concrete : Correlation with Some Measures of Fiber Spacing, *ACI Material Journal*, V 87, No.5, Sept-Oct.
- Li, V.C., et al 1998. Influence of Fiber Bridging on Structural Size-effect, *Int. Journal of Solids Structures*, Vol. 35: 4223-4238